processes

MDPI

Article

Carbonaceous Adsorbents Derived from Agricultural Sources for the Removal of Pramipexole Pharmaceutical Model Compound from Synthetic Aqueous Solutions

Efstathios V. Liakos [1], Kyriazis Rekos [2], Dimitrios A. Giannakoudakis [3], Athanasios C. Mitropoulos [1] and George Z. Kyzas [1,*]

[1] Department of Chemistry, International Hellenic University, GR-654 04 Kavala, Greece; stathilas@gmail.com (E.V.L.); amitrop@chem.ihu.gr (A.C.M.)
[2] Department of Chemistry, Aristotle University of Thessaloniki, GR-541 24 Thessaloniki, Greece; rekoskyriazis@yahoo.gr
[3] Institute of Physical Chemistry, Polish Academy of Sciences, Kasprzaka 44/52, 01-224 Warsaw, Poland; dagchem@gmail.com
* Correspondence: kyzas@chem.ihu.gr; Tel.: +30-2510-462218

Abstract: The aim of the present study was to synthesize various samples of activated carbon (AC) from different agricultural sources as precursors, like orange peels, tea stalks, and kiwi peels, as well as sucrose. The synthesis of AC was achieved with chemical activation using H_3PO_4 and KOH. The produced AC samples were tested as adsorbents for the removal of a pharmaceutical model compound, pramipexole dihydrochloride (PRM), from synthetic aqueous synthetic solutions. The produced-from-sucrose AC presented the higher yield of synthesis (~58%). The physicochemical features of the materials were analyzed by FTIR spectroscopy, N_2 physisorption, and SEM imaging. More specifically, the AC sample derived from sucrose (SG-AC) had the highest specific surface area (1977 m^2/g) with the total pores volume, mesopores volume, and external surface area being 1.382 cm^3/g, 0.819 cm^3/g, and 751 m^2/g, respectively. The effect of the initial pH and PRM concentration were studied, while the equilibrium results (isotherms) were fitted to Langmuir and Freundlich models. The maximum adsorption capacities were found to be 213, 190, 155, and 115 mg/g for AC samples produced from sucrose, kiwi peels, orange peels, and tea stalks, respectively.

Keywords: activated carbons; adsorption; pharmaceuticals; sucrose; kiwi peels; orange peels; tea waste

Citation: Liakos, E.V; Rekos, K.; Giannakoudakis, D.A; Mitropoulos, A.C; Kyzas, G.Z Carbonaceous Adsorbents Derived from Agricultural Sources for the Removal of Pramipexole Pharmaceutical Model Compound from Synthetic Aqueous Solutions. *Processes* **2021**, *9*, 253. https://doi.org/10.3390/pr9020253

Academic Editor: María V. López-Ramón
Received: 30 December 2020
Accepted: 25 January 2021
Published: 29 January 2021

1. Introduction

Activated carbons (ACs) is a class of materials with excellent adsorption capability [1–5], high specific surface area [6–9], and total pore volumes [10–13], where according to its porous structure it can be separated depending on the diameters of pores in microporous (0–2 nm), mesoporous (2–50 nm), and macroporous structures (>50 nm), respectively [6]. It is important to highlight the definition of activated carbon; it is a carbon-rich solid that is derived from biomass or other carbonaceous substances, using pyrolysis. In the process, a carbon material is also "activated" by processes that greatly increase the surface area of the material, allowing it to capture (or "adsorb") a larger quantity of molecules. This high adsorption capability allows activated carbon to be effective at removing contaminants from water and air, which is why activated carbon is typically intended for remediation or purification projects. So, the key factor in the use of activated carbon in remediation/decontamination technologies is to use the most appropriate primary source so as to prepare the AC with the highest specific surface, suggesting the highest decontaminative ability. For this reason, various agricultural peels (biochars) were tested as adsorbents [14] and also the preparation tips to synthesize the most suitable activated carbon sample [15].

In the last decades, the pollution of the aquatic environment with micropollutants, predominately due to the rise of industrialization, has increased the environmental concern. These emerging contaminants can be categorized based on their origin in natural and anthropogenic substances, with the major ones of the latter category including pesticides, pharmaceuticals, industrial chemicals, steroids hormones, products for personal care, and many other types of emerging compounds. Their diversity and low concentration complicate the procedures of analysis and detection, with the result being the creation of challenges for the processes of wastewater treatment [16].

There are a wide number of methods for the treatment of water and wastewater, including reverse osmosis [17], filtration with membranes [18], ion-ion exchange [19], photocatalytic detoxification [20], and so on, but it cannot be omitted that these techniques have many drawbacks. However, adsorption is a very efficient process in a variety of cases compared to the aforementioned techniques, because a plethora of organic pollutants simultaneously with inorganic ones can be removed from aqueous matrixes [21–24]. Additionally, the absence of sludge formation, the potential reusability of the adsorbents, the operation simplicity, and the low costs when compared with other processes must also be noted [25]. Going a step beyond towards sustainable approaches, the synthesis of activated carbons can be achieved in large scales by utilizing abundantly available biomass/wastes as feedstocks.

The advantages of chemical activation include activation in a shorter duration with a single activation step, lower temperature of activation (lower energy and operating costs), higher yields, and as a result higher atom economy, resulting in high specific surface area and microporosity. The method of chemical activation also has disadvantages, such as the high cost for the purchase of activating agents, and the amount of deionized water that is used in order to remove process-generated impurities. Phosphoric acid (H_3PO_4) has been preferred and is suitable for the process of chemical activation, a fact that is attributed to economic and environmental concerns. In addition, the use of H_3PO_4 can lead to the development of both a micropores and mesopores structure in the yielding ACs [26]. Potassium hydroxide (KOH) activation agent is also widely utilized because it can produce ACs of a high volume in pores and especially in a microporous structure of elevated specific surface area, reaching values above 3000 m^2/g. The process of activation with KOH is efficient for the formation from small mesopores to ultra-micropores into the framework of carbon fibers, carbon nanofibers, carbons derived from carbide, carbon aerogels, carbon nanotubes, and templated graphene [27].

In this present work, the synthesis of ACs from various biomass sources (sucrose, kiwi peels, orange peels, and tea stalks) and by using H_3PO_4 and KOH as activation agents was investigated in order to obtain efficient removal medias against pramipexole dihydrochloride from aqueous solution.

Pramipexole dihydrochloride is a pharmaceutical compound ((6S)–N6-propyl-4,5,6,7-tetrahydro-1,3-denzothiazole-2,6-diamine) and is an innovative and non-ergoline dopamine agonist. Primarily, this pharmaceutical compound was used against the idiopathic Parkinson's disease symptoms [28–30], and also during research in Europe and the US, its usage was approved in adults for the treatment of the syndrome of idiopathic restless legs [31]. Consequently, due to its unique activity, it is widely used at a worldwide scale as a pharmaceutical compound. Moreover, it can be assumed that the use of this pharmaceutical compound will continue to develop and increase when the physicians of primary care become more familiar with its use. Some hospitals and industries that produce this pharmaceutical compound are discharging this pharmaceutical compound in their effluents, resulting in the final recipient being the natural resources of water. It is important to note that until now, no data is given in the literature for the detection of prami in water/wastewater. However, as described above, pramipexole has similar groups with other pharmaceutical compounds, so the study of its removal from aqueous systems can be a good tool for explanations. So, the treatment of wastewater that contains pramipexole is of great interest [28].

The selection of the sources to produce the activation carbons and the reasons behind were based on the following: (i) one of the most valuable agricultural wastes for the synthesis of AC is orange peels, which are mainly discarded in large quantities from juice industries. The pollution of land space with orange peels is becoming problematic due to the phenolic functional groups [32,33]; (ii) one of the most widely consumed beverages is tea, and it is consumed on a daily basis all around the world [34]. The tea wastes are not useful in any area of industrial activity and can be used probably only as fertilizers; (iii) kiwi peels were selected because they have high cellulose content; and (iv) sucrose (α-D-glucopyranosyl-(1→2)-β-D-fructofuranoside) is an inexpensive chemical produced by sugar cane and sugar beet cultivation, having a lot of carbons in its structure. After the optimization of synthetic protocols, the AC samples were characterized with FTIR spectroscopy, N_2 physisorption tests, and scanning electron microscopy (SEM) images. The removal efficiency evaluation was conducted based on the maximum theoretical adsorption capacity, which was calculated by fitting the equilibrium data to Langmuir and Freundlich models.

2. Materials and Methods

2.1. Materials

The model pollutant used to simulate the pharmaceutical wastewater was pramipexole dihydrochloride ($C_{10}H_{21}Cl_2N_3OS$; MW = 324.44 g/mol, assay 99.2%), which was purchased by the pharmaceutical company Amino Chemical Ltd. (Marsa, Malta). Figure 1 presents the chemical structure of pramipexole dihydrochloride. The synthetic pharmaceutical solutions (1000 mg/L) were synthesized by weighing and diluting the appropriate quantity of pramipexole in water solution. In addition, for the assessment of those solutions, spectrophotometric assays were used and it was determined that after their storage at −20 °C, the overall concentration at the prepared solution can stay stable longer than 1 week.

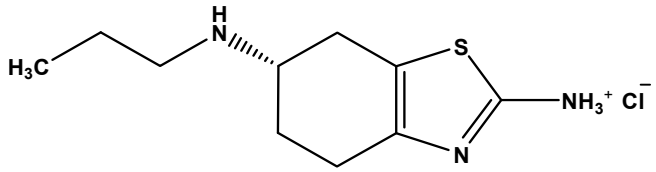

Figure 1. Chemical structure of pramipexole dihydrochloride.

The carbon precursors for the production of activated carbon were sucrose (commercial product), orange and kiwi peels (residues from Greek restaurants), and tea stalks (supplied by Department of Forestry and Natural Environment, International Hellenic University, Thessaloniki, Greece). All the chemical agents used for the synthesis of AC, including H_3PO_4, KOH, and HCI, were purchased from Sigma-Aldrich (St. Louis, MO, USA) and were of analytical grade.

2.2. Synthesis of AC from Various Carbon Sources

2.2.1. Activated Carbon from Sucrose (SG-AC)

Sucrose (SG) was used for the synthesis of SG-AC. The SG was placed in a pestle and crunched in order to obtain a fine powder. The activation was carried out with using phosphoric acid. Briefly, 10 g of fine SG powder were dispersed in 10 mL of deionized water placed in a vial and kept at 65 °C under stirring for 5 min. Then, 17 mL of H_3PO_4 (85% *w*/*w*) were added and the solution was kept at the same temperature under stirring for 45 min. During the preparation process, the color of the suspension changed from white initially to yellow and then to blackish. Finally, the mixture was swollen and stabilized when the temperature of suspension was adjusted at 120 °C. The obtained swollen stable product was placed in porcelain boats and completely dried for 1.5 h at 140 °C. The yielded material after the drying process had a powder form. The process of carbonization and

activation was achieved in a pyrolysis oven at 650 °C for 1 h (heating rate 10 °C/min), under N_2 (pure: 99.9%; flow: 30 STP cm^3/min). The yielded material was cooled down at ambient temperature and thereafter was washed with HCl (37%) in order to remove the excess H_3PO_4 and then washed with deionized water until reaching the neutral pH (6–7) of the filtrate. Finally, the material was placed in an oven and dried at 110 °C for 12 h to obtain the final black powder, referred to as SG-AC.

2.2.2. Activated Carbon from Orange Peels (ORP-AC), Tea Stalks (TEA-AC), and Kiwi Peels (KWP-AC)

The orange peels (ORP) were washed with deionized water to remove the inorganic impurities. Then, they were dried at 110 °C (24 h) in an oven to eliminate the moisture. Next, the obtained biomass was ground using a mortar and sieved to obtain particles with a size of 0.45–0.15 mm. The ORP biomass was chemically activated by using KOH. In particular, 10 g of dry ORP were mixed for 24 h with an aqueous basic solution (3 M KOH) under stirring at ambient temperature. Afterwards, the obtained chemically treated biomass was dried in an oven at 110 °C (24 h). The process of carbonization/activation was achieved by thermally treatment of the obtained solid residues at 650 °C (heating rate 10 °C/min) for 1.5 h, under N_2 (99.999% pure) flow of 30 STP cm^3/min. After cooling down at ambient condition, the received orange peels derived activated carbon was washed with HCl (37%) solution and water until neutral pH (6–7) of the filtrate in order to remove the excess KOH and impurities. Finally, the yielded black material was dried at 110 °C (24 h), with the final dry sample referred to as ORP-AC.

Activated carbon from tea stalks was prepared following the same synthetic protocol but using 10 g of tea stalks (TEA) as a precursor instead of orange peels, while the final obtained material is referred to as TEA-AC. For the kiwi peels-derived material, 10 g of dry KWP were treated as for ORP or TEA in order to obtain the dried and ground/powder biomass, which was dispersed in 125 mL of H_3PO_4 (85% *w*/*w*) for 24 h under vigorous stirring at ambient conditions, instead of a basic solution, with the rest of the steps being identical to those for ORP-AC. The kiwi peels-derived activated carbon is referred to as KWP-AC. A schematic illustration for the main steps of the synthetic protocols can be seen in Figure 2.

2.3. Adsorption Evaluation

2.3.1. pH Effect

The adsorption evaluation was achieved by studying the effect of the initial pH and by the analysis of the obtained isotherms. All the batch experiments were performed in triplicates. For the pH-effect experiment, a fixed amount of AC sample (0.02 g) was added to 20 mL of pramipexole dihydrochloride (PRM) solution (C_0 = 200 mg/L) in a conical flask. The pH adjustment (at pH = 3, 5, 7, 9, 11) of the solution was achieved with micro-additions of HCl (0.01 M) or NaOH (0.01 M) aqueous solutions. Then, the flasks of different solution pH were placed in a shaking bath (25 °C) with a fixed agitation speed (160 rpm) and allowed to shake for 24 h. Finally, the analysis of the residual PRM concentration was carried out.

2.3.2. Equilibrium/Isotherms

For the isothermal experiments, a fixed amount of AC sample (0.02 g) was added to 20 mL of PRM solution (C_0 = 5–250 mg/L) in a conical flask. The initial pH adjustment of the solution at pH = 3 (since it was found to be the optimum value from Section 2.3.1) was achieved with micro-additions of HCl solution (0.01 M) or NaOH (0.01 M). Then, the flasks of different initial PRM concentrations were placed in a shaking bath (25 °C) with a fixed agitation speed (160 rpm) and allowed to shake for 24 h. Finally, the analysis of the residual PRM concentration was carried out.

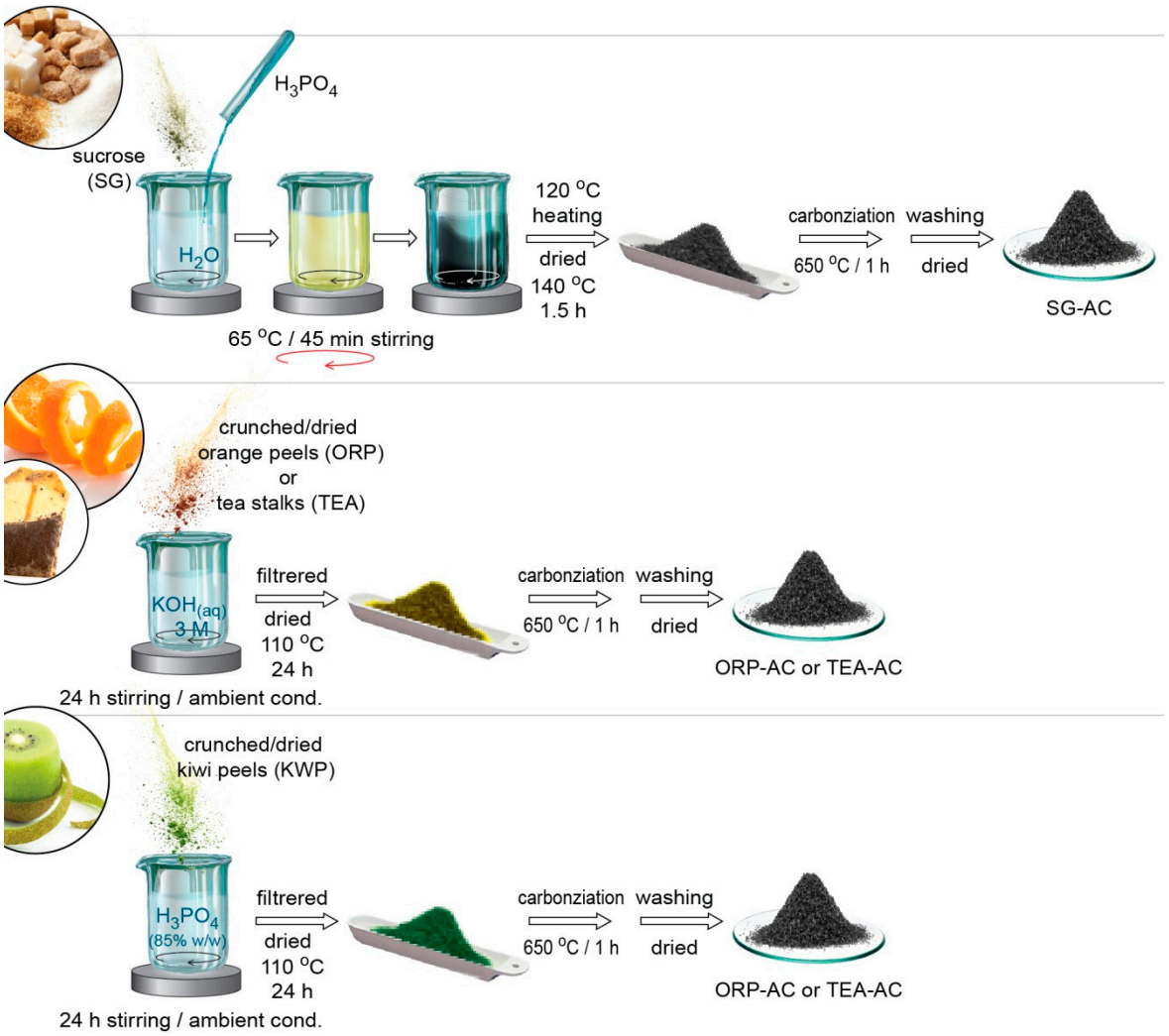

Figure 2. Synthesis procedure of activated carbon (AC) samples.

The first stage in a lab-scale adsorption experimental design is the pH-effect experiments. This is very important in order to understand the adsorption interactions at the optimum pH conditions. This is crucial for the study of the whole adsorption phenomena. It must be noted that, in some cases, the optimum pH conditions are not the same as those of the discharging effluent. In general, the composition of pharmaceutical wastewater is complex, which has a high concentration of organic matter, microbial toxicity, high salt, and it is hard to biodegrade. In addition, most pharmaceutical factories use the batch process, and there are different raw materials and production processes, which causes huge varieties in different wastewater with pH values from 1 to 8 [35,36]. However, the latter (different optimum pH value in the lab scale compared to the pH of real wastewater) can be overcome with the (i) adjustment of the pH value of the real effluent or (ii) with further attempts to synthesize adsorbent materials, which successfully act both at the optimum pH conditions in batch mode (lab scale) and in real conditions (with probably a slight decrease). Especially regarding the pH adjustment of the real effluent, the adjustment of pH in real wastewaters is not usually a good method, especially in domestic wastewater treatment plants (WWTPs). However, there is no clear indication about the pH conditions of wastewaters from pharmaceutical industries. There are reports in the literature with pH values in acidic conditions and also some other studies with alkaline pH values [35,36]. The latter depends on the number and nature (charge) of the pharmaceutical compounds existing in the effluent.

2.3.3. Analysis and Fitting

The concentration of residual PRM was determined with the use of the spectrophotometric method by adjusting its UV absorbance at λ_{max} = 263 nm with the use of a UV-Vis spectrophotometer (U-2000, Hitachi, Japan). The absorbance wavelength change that was obtained from the generated results was determined as unimportant (~2%). The calibration curves were created from absorbance versus PRM concentration using the linear Beer–Lambert relationship. To correlate the absorbance measured from UV-Vis spectrophotometer with the PRM concentration, the following chart was prepared (calibration curve) (Figure 3).

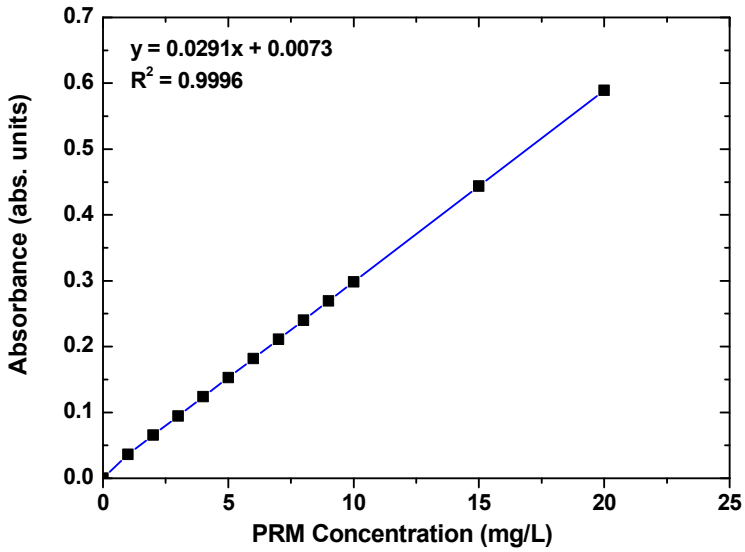

Figure 3. Calibration curve of pramipexole dihydrochloride (PRM).

In addition, with the use of the mass balance equation, as presented below (Equation (1)), the quantity of pramipexole that is taken up at the equilibrium phase was calculated Q_e (mg/g) (where C_0 and C_e (mg/L) are the initial and equilibrium concentrations of PRM, respectively; V (L) is the volume of aqueous solution; and m (g) is the mass of the AC sample used):

$$Q_e = \frac{(C_0 - C_e)V}{m} \quad (1)$$

The experimental equilibrium data were fitted to the Langmuir (Equation (2)) [37] and Freundlich (Equation (3)) [38] isotherm equations expressed by the following equations:

$$Q_e = \frac{Q_m K_L C_e}{1 + K_L C_e} \quad (2)$$

$$Q_e = K_F C_e^{1/n} \quad (3)$$

where Q_m (mg/g) is the maximum amount of adsorption; K_L (L/mg) is the Langmuir adsorption equilibrium constant; K_F ($mg^{1-1/n}$ $L^{1/n}$/g) is the Freundlich constant representing the adsorption capacity; and n (dimensionless) is the constant depicting the adsorption intensity.

2.3.4. Error Analysis

Determination of the best isotherm model is only possible through analysis of the correlation coefficient (R^2). Although efficient, this indicator is limited to solving isotherm models that present linear forms. Therefore, in this work, three different error functions were employed in order to discover the isotherm model most suitable for representing the experimental data. The sum of squared errors (SSEs) (Equation (4)) is the most commonly

utilized error function. However, it has the disadvantage of providing isotherm parameters that present better adjustment to the final portion of the isotherm. This is due to the magnitude of the errors, which causes an increase in squared errors as the adsorbate concentration increases. The sum of absolute errors (SAE) (Equation (5)) also provides better adjustments for higher concentrations. This occurs because an increase of the concentration range causes an increase in error. The average relative error (ARE) (Equation (6)) function attempts to minimize the fractional error distribution across the entire concentration range:

$$SSE = \sum_{i=1}^{n} \left(Q_{e,calc} - Q_{e,exp} \right)_i^2 \quad (4)$$

$$SAE = \sum_{i=1}^{n} \left| Q_{e,calc} - Q_{e,exp} \right|_i \quad (5)$$

$$ARE = \frac{100}{n} \sum_{i=1}^{n} \left| \frac{Q_{e,calc} - Q_{e,exp}}{Q_{e,exp}} \right|_i \quad (6)$$

2.4. Characterization Techniques

The morphology of the synthesized AC samples was studied by scanning electron microscopy (SEM) images by a Jeol JSM-6390 LV, Japan. The accelerating voltage was 15.00 kV, and the scanning was performed in situ on a dry sample powder. For the FTIR spectra (after adsorption of the anti-inflammatory compounds), an FTIR-spectrometer (Perkin Elmer FT-IR/NIR spectrometer Frontier, New York, NY, USA) was used. The spectra were recorded from 3500 to 500 cm^{-1} (2 cm^{-1} as the resolution and a total of 32 scans) and presented with baseline correction (transmittance mode). The specific surface area of ACs was estimated at 77 K from the nitrogen adsorption/desorption isotherms by employing a Quantachrome analyzer (Nova 4200e, New York, NY, USA). The model of Brumauer–Emmett–Teller (BET) was used in order to calculate the BET specific surface areas. The calculation of the external surface area, micropore surface area, and micropore volume was achieved with the *t*-plot method.

3. Results and Discussion

3.1. Characterizations

3.1.1. FTIR Spectroscopy

Figure 4a collects the FTIR spectra of all herein synthesized AC samples. SG-AC appears as a weak band at about 2285 cm^{-1}, which is assigned to the P–H bond, and indicates the presence of phosphine and phosphonate structures [39]. The broad peaks at about 2077 and 1987 cm^{-1} are assigned to N–H$\cdots$O stretching and bending intramolecular hydrogen bonding. The broad band centered at 1902 cm^{-1} is attributed to the stretching and bending vibrations of N–H$\cdots$O and may suggest the appearance of intramolecular hydrogen bonding [40]. The broad band at 1554 cm^{-1} corresponds to the C=O stretching vibration [41] in the carboxyl groups [42] or lactose groups [43] or to the skeletal C=C vibration of aromatic rings [44]. Moreover, the broad band at 1150 cm^{-1} is attributed to –OH stretching and bending vibrations in C–OH, respectively [28]. Moreover, the weak band at 877 cm^{-1} corresponds to the out-of-plane bending mode of the group of C–H or O-H [41] and the very weak band at 613 cm^{-1} is ascribed possibly to O–H vibrations in the OH groups [40] of aromatic structures [26].

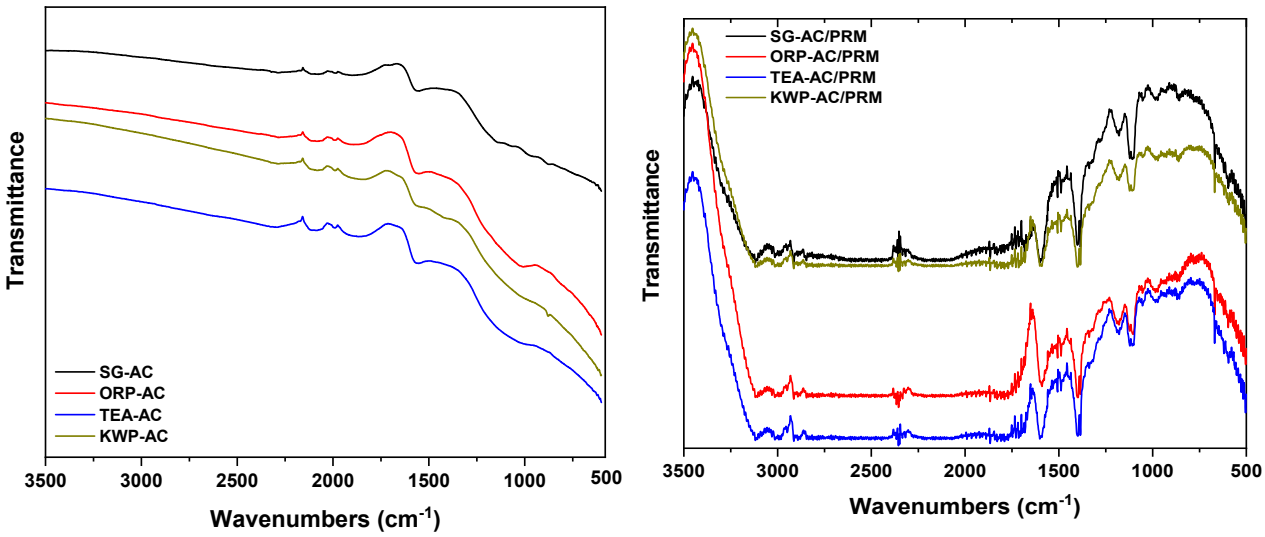

Figure 4. FTIR spectra of the prepared AC samples (**a**) before PRM adsorption and (**b**) after PRM adsorption.

In the case of ORP-AC, the FTIR spectrum presents a weak band at about 2286 cm^{-1}, which is assigned to the P–H bond and indicates the presence of phosphine and phosphonate structures [39]. The broad peaks at about 2083 and 1992 cm^{-1} are assigned to N–H···O stretching and bending intramolecular hydrogen bonding. In addition, the broad band at 1892 cm^{-1} can be attributed to the stretching and bending vibrations of N–H···O and may suggest the appearance of intramolecular hydrogen bonding [40]. The broad band at 1551 cm^{-1} may be assigned to the skeletal C=C vibration of aromatic rings [40,44]. The broad band at about 1007 cm^{-1} is associated with the C–O stretching of benzyl hydroxyl [45]. Moreover, the weak band at 876 cm^{-1} corresponds to the out-of-plane bending mode of the group of C–H or O–H [41] and the very weak band at 614 cm^{-1} is ascribed possibly to ν O–H in the OH groups [40] of aromatic structures [26].

In the case of TEA-AC, the FTIR spectrum presents a broad band at about 2295 cm^{-1}, which is assigned to the P–H bond and indicates the presence of phosphine and phosphonate structures [39]. The broad peaks at about 2084 and 1992 cm^{-1} are assigned to N–H···O stretching and bending intramolecular hydrogen bonding. In addition, the broad band at 1866 cm^{-1} is attributed to the stretching and bending vibrations of N–H···O and may suggest the appearance of intramolecular hydrogen bonding [40]. The broad band at 1552 cm^{-1} may be assigned to the skeletal C=C vibration of aromatic rings [40,44] or to the benzene ring stretch [45]. Moreover, the broad band at 1150 cm^{-1} is attributed to –OH stretching and bending vibrations in C–OH, respectively [28]. Moreover, the weak band at 877 cm^{-1} corresponds to the out-of-plane bending mode of the group of C–H or O–H [41] and the very weak band at 615 cm^{-1} is ascribed possibly to νO-H in the OH groups [40] of aromatic structures [26].

In the case of KWP-AC, a weak band at about 2287 cm^{-1} is assigned to the P–H bond and indicates the presence of phosphine and phosphonate structures [39]. The broad peaks at about 2085 and 1988 cm^{-1} are assigned to N–H···O stretching and bending intramolecular hydrogen bonding. In addition, the broad band at 1842 cm^{-1} is attributed to the stretching and bending vibrations of N–H···O and may suggest the appearance of intramolecular hydrogen bonding [40]. The broad band at 1552 cm^{-1} may be assigned to the skeletal C=C vibration of aromatic rings [40,44]. In addition, the broad band at 1150 cm^{-1} is attributed to –OH stretching and bending vibrations in C-OH, respectively [28]. Moreover, the weak band at 878 cm^{-1} corresponds to the out-of-plane bending mode of the group of C–H or O-H [41] and the very weak band at 612 cm^{-1} is ascribed possibly to νO–H in the

OH groups [40] of aromatic structures [26]. All the above bands based on different bonding are summarized in Table 1.

Table 1. FTIR bands based on different bonding.

	Wavelength (cm^{-1})			
Bond/Vibration	**SG-AC**	**ORP-AC**	**TEA-AC**	**KWP-AC**
P–H	2285	2286	2295	2287
N–H O	2077, 1987, 1902	2083, 1992, 1892	2084, 1992, 1866	2085, 1988, 1842
C=O or C=C *	1554	1551 *	1552	1552 *
–OH in C-OH	1150		1150	1150
C–O		1007		
C–H or O–H (out-of-plane bending)	877	876	877	878
νO–H in OH (aromatic structures)	613	614	615	612

* refers to C=C.

To understand the adsorption interaction among PRM molecules and materials, FTIR spectra after adsorption were taken. So, after PRM adsorption, the band at about 2285 cm^{-1} revealed a higher intensity, while a new band at about 2360 cm^{-1} appeared (Figure 4b). These findings are attributed to the interaction with PRM molecules. In addition, the band at 1552 cm^{-1} became more intense and a new band at 1600 cm^{-1} appeared. On the other hand, the bands at 2077, 1987, and 1902 were eliminated, depicting that these groups reacted with the PRM molecule. The bands at 878 (out-of-plane bending) and 612 cm^{-1} (νO–H) shifted to 865 and 672 cm^{-1}, respectively.

3.1.2. N_2 Physisorption Tests Analysis

Nitrogen adsorption/desorption isotherms at −196 °C for the prepared AC samples are presented in Figure 5a.

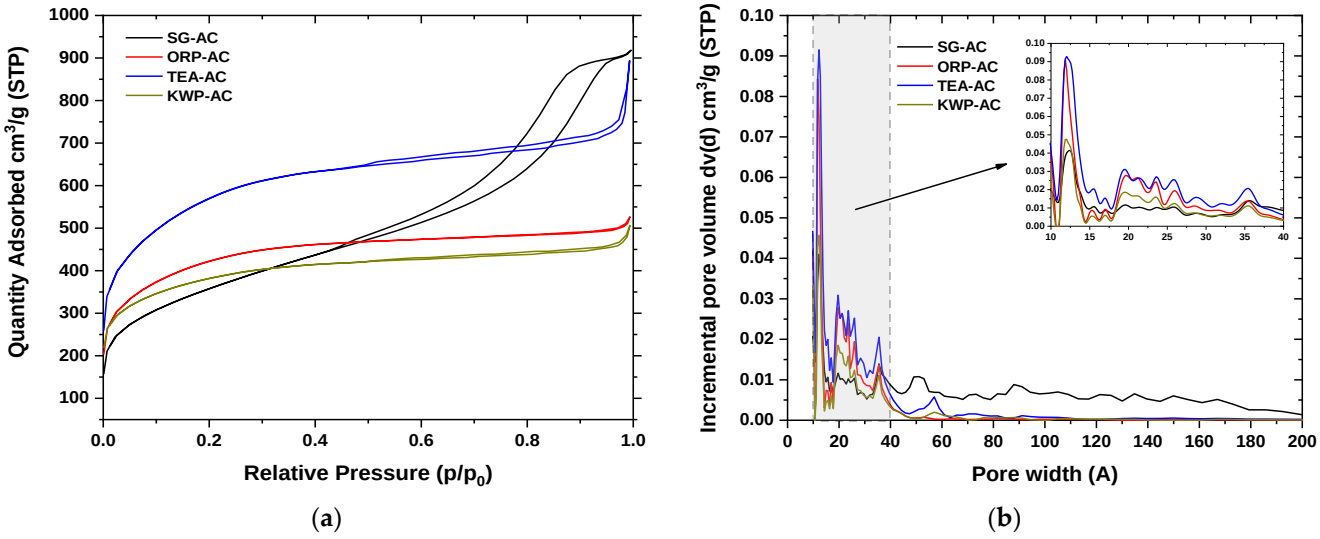

Figure 5. (**a**) Nitrogen physisorption isotherms of the prepared AC samples; (**b**) Pore size distributions for the prepared AC samples.

According to the classification of IUPAC, the adsorption isotherms for ORP-AC, TEA-AC, and KWP-AC revealed combined Type I isotherm characteristics at very low relative pressure p/p_0 and Type II characteristics at high relative pressure p/p_0, indicating the presence of micropores and mesopores at <2 and 2–50 nm, respectively. These results were also confirmed due to the presence of H_3 and H_4 desorption hysteresis loops, which associated with slit-shaped pores [32]. In contrast, SG-AC presented a Type IV isotherm [46–48] and presents a desorption hysteresis loop of Type H_2(b), because its desorption branch is

not too steep as in the case of H_1 and H_2(a) hysteresis loops. Such hysteresis loop results are mainly presented after hydrothermal treatment of certain mesoporous ordered silicas and mesocellular silica foams [49]. According to the classification of IUPAC, the Type IV isotherm is exhibited when a mixture of microporous and mesoporous material occurs. This indicates capillary condensation in the mesopores structure [50]. All the details about the textural parameters of the yielded AC samples are given in Table 2.

Table 2. Details of the textural parameters of the yielded AC samples.

AC Sample	Surface Area (m^2/g)	Micropore Surface Area (m^2/g)	External Surface Area (m^2/g)	Total Pore Volume (cm^3/g)	Micropore Volume (cm^3/g)	Mesopore Volume (cm^3/g)
SG-AC	1977	1226	751	1.382	0.563	0.819
ORP-AC	1298	340	928	1.421	0.152	1.270
TEA-AC	1284	922	361	0.784	0.439	0.345
KWP-AC	1446	976	471	0.815	0.454	0.361

As it can be seen from Table 2, the highest total pore volume (1.421 cm^3/g) and mesopores volume (1.270 cm^3/g) was found for ORP-AC, while the highest surface area was found for SG-AC (1977 m^2/g). In addition, the highest external surface area (928 m^2/g) and micropore surface area (1226 m^2/g) were achieved for ORP-AC and SG-AC, respectively. The lowest micropore volume was found for ORP-AC (0.152 cm^3/g), while the highest micropore volume was achieved with SG-AC (0.563 cm^3/g).

Special attention must be given to pore size distributions. The pores of ORP-AC, TEA-AC, and KWP-AC are located between the 18 and 37 Å width range (Figure 5b). In addition, TEA-AC and ORP-AC have the higher incremental pore volume of 0.091 and 0.084 $cm^3/Å/g$, respectively (between 10 and 18 Å).

Regarding KWP-AC, the incremental pore volume is 0.045 $cm^3/Å/g$ in the range 10–18 Å. The highest incremental pore volume (0.0074 $cm^3/Å/g$) was presented for SG-AC at about 40–100 Å, while for all other cases, it is almost zero. SG-AC presents an increase of incremental pore volume at 80–170 Å of approximately 0.0096 $cm^3/A/g$ (mesoporous structure), while in the other cases, it is near zero. This result may be attributed to the high surface area (1976.817 m^2/g) of SG-AC, high total pore volume (1.3820 cm^3/g) and mesopore volume (0.8190 cm^3/g), and also due to the combination of the micropores (~40.7%) and mesopores structure (~59.3%).

It must be noted that some changes are attributed to the different synthesis route that was followed. Hence, the development of the micropore volume is similar according to the solid salt volume, which is incorporated into the particle, and has as a result a uniform structure of microporosity [51]. In the case of chemical activation with H_3PO_4, volatile phosphorus compounds can be formed due to the following reactions [44]:

$$\begin{gathered} 4H_3PO_4 + 10C \rightarrow P_4 + 10CO + 6H_2O \\ 4H_3PO_4 \rightarrow P_4O_{10} + 6H_2O \\ P_4O_{10} + 10C \rightarrow P_4 + 10CO \end{gathered} \quad (7)$$

In the case of chemical activation with KOH, the pores formation is attributed to the metallic potassium intercalation process. The activation process is as follows [52]:

$$\begin{gathered} 6KOH + 2C \rightarrow 2K + 3\,H_2 + 2K_2CO_3 \\ K_2CO_3 \rightarrow K_2O + CO_2 \\ K_2CO_3 + 2C \rightarrow 2K + 3CO \\ CO_2 + C \rightarrow 2CO \\ C + K_2O \rightarrow 2K + CO \end{gathered} \quad (8)$$

3.1.3. SEM Images

Figure 6 presents the SEM images of the prepared AC samples. It can be clearly observed that the AC derived from sucrose (Figure 6a) has particles of a very small size (5–40 µm), which may be attributed to the fact that during the process of impregnation with H_3PO_4, a small amount of monosaccharides did not achieve aggregation with the other monosaccharides for the achievement of a solid surface. It can also be observed from Figure 6b–d that ORP-AC, TEA-AC, and KWP-AC have a rough surface while many cages and cavities can be observed that can be linked to the entrance of the porous network. This fact is attributed to the intercalation of metallic potassium in the cellulosic (33.98%) and pectin (20.9%) structure of the orange peels biomass [53], cellulose, and lignocellulose structure [54]. The cavities produced from the space, which was previously occupied by KOH due to the impregnation process, thereafter were evaporated (volatiles) due to the process of carbonization. Then, the inert atmosphere (N_2 flow) and the carbonization process at high temperature, which was initially followed by the impregnation of raw sample (ORP, TEA) with the KOH activation agent, presented favorable microstructure degradation. So, it can be concluded that such microstructure degradation is related when important losses of mass occur.

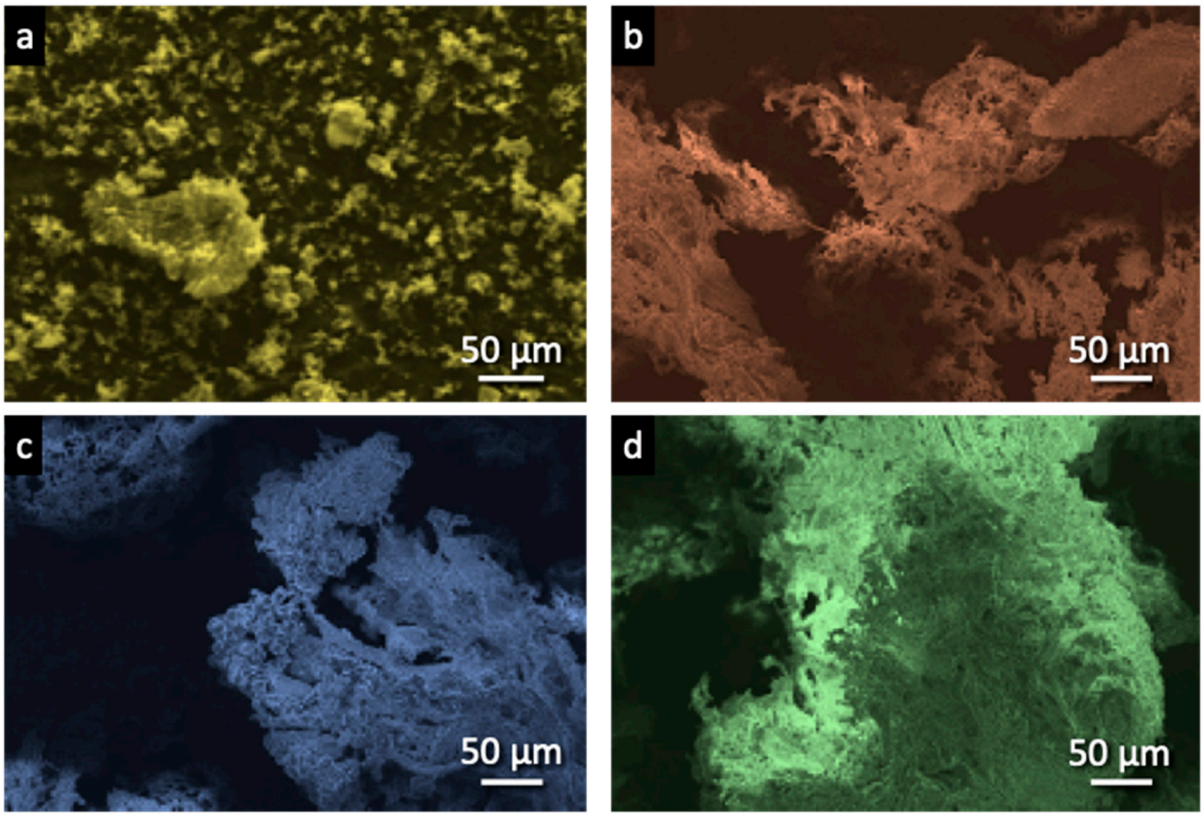

Figure 6. Activated carbon samples derived from (**a**) sucrose, (**b**) orange peels, (**c**) tea stalks, and (**d**) kiwi peels.

3.1.4. Yield of AC Samples

The yield of SG-AC was found to be as high as 58%. So, to understand this, a special note must be made for the whole activation process. The phosphorus of H_3PO_4 is intercalated in the molecular structure of broken down carbon rings of fructose (ketose-$C_6H_{12}O_6$) and glucose (aldose-$C_6H_{12}O_6$) with a mild exothermic reaction at approximately 120 °C. The phosphorus moieties are intercalated efficiently within and between the molecular structure of the carbon rings of fructose (ketose-$C_6H_{12}O_6$) and glucose (aldose-$C_6H_{12}O_6$) due to the high solubility of monosaccharides in water solutions and the existence of tem-

perature. More specifically, after the addition of phosphorus in the water solution, this mild exothermic reaction at 120 °C breaks down the carbon rings of fructose (ketose-$C_6H_{12}O_6$) and glucose (aldose-$C_6H_{12}O_6$), due to dehydration of the hybridized orbitals between carbon atoms (sigma bonds). The dehydration of sucrose with H_3PO_4 gives a high yield of AC (58%), because after the dehydration process, the –OH and –HO bonds of sucrose are replaced by the –OH and –HO bonds of phosphoric acid, and consequently are intercalated and the phosphorus compounds in the molecular structure of atom of carbon create a regeneration of "new sucrose", because the sucrose and phosphoric acid have the same crystal structure (monoclinic).

After the oven-dry process, the yielded amount of carbon from 10 g of initial precursor (sucrose) was 32 g. It is important to note that 10 g of sugar gave 32 g after the impregnation with H_3PO_4 and drying in an oven at 140 °C for 1 h. This is attributed to the nature of sucrose, because it is "disaccharide", and the phosphorus compound breaks down the aromatic rings between the carbon atoms, causing the increase (320%) of the initial weight. In addition, another advantage due to the intercalation of phosphorus compounds in the molecular structure of excess break down of carbon rings, due to dehydration of hybridized orbitals, is that it does not generate high amounts of volatile gases during the process of pyrolysis and consequently a high amount of AC is produced. After the process of pyrolysis at 650 °C in an N_2 atmosphere, the weight of AC was 18.1 g. This result may be attributed to, in cooperation with the previous (32 g), the breakdown of carbon rings of fructose (ketose-$C_6H_{12}O_6$) and glucose (aldose-$C_6H_{12}O_6$), due to dehydration of the hybridized orbitals between carbon atoms. However, after the process of washing (decantation) in order to obtain an almost neutral pH (6–7), the obtained material had a final weight of approximately 5.8 g. As it can be observed in Figure 7, the other AC samples had very low yields of AC due to the increased value of volatile gases from the surface of carbon during pyrolysis.

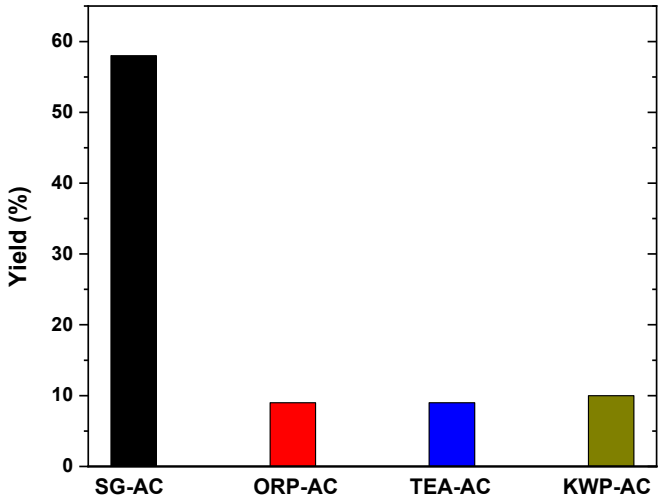

Figure 7. Yield (%) of the prepared AC samples.

3.2. Adsorption Evaluation

3.2.1. Effect of pH

Figure 8 shows the removal efficiencies of activated carbons over a pH range of 3–11. It can be concluded that the optimum PRM removal is achieved at pH 3 for all AC samples.

It is important to note that PRM was experimentally found to be stable and not hydrolyzed at this pH (3). The latter was found carrying out a hydrolysis experiment (10.00 mg/L of PRM in deionized water adjusted at pH = 3 with shaking at 25 °C for 24 h—given that this was the maximum contact time in adsorption); the concentration found was 9.86 mg/L, which means 1.4% as a hydrolysis percentage. Additionally, the scanning of the PRM in UV-Vis did not reveal any change in λ_{max} (263 nm) (Figure 9).

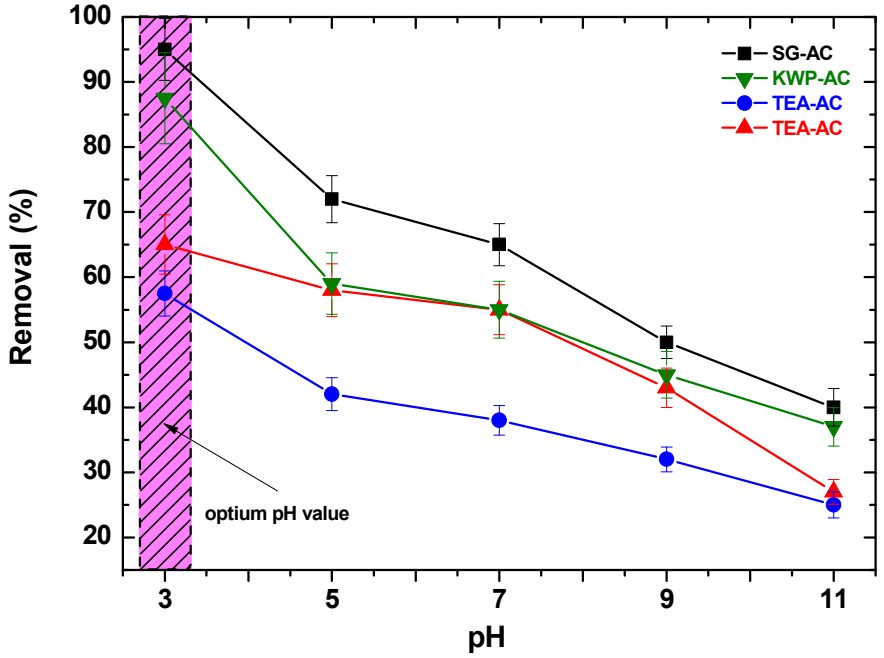

Figure 8. Effect of pH for the removal of PRM from aqueous solutions.

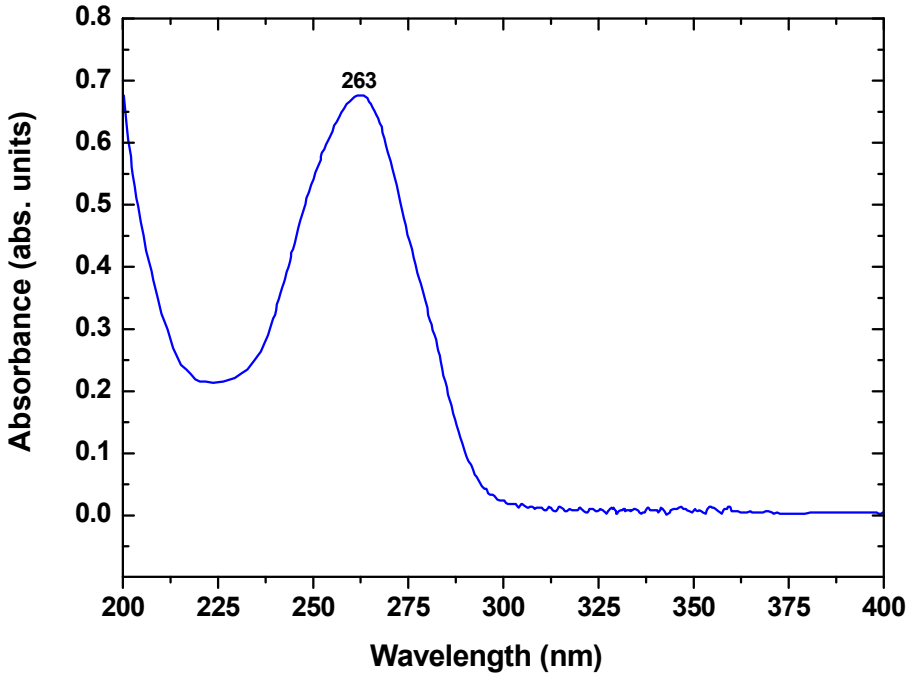

Figure 9. UV-Vis spectrum of PRM after 24 h (hydrolysis experiment).

Another reason for the observed effect of pH on the adsorption may be the suppression of the complexation. In solutions with a low pH value, some functional groups are protonated (or difficult to dissociate) and the complexation between PRM and the functional groups on the surfaces of the activated carbons increases. Additionally, based on the above FTIR results, it can be concluded that strong pi-pi electron coupling and/or stacking (mainly dispersion forces) between PRM molecules and aromatic rings of the carbon may be the adsorption mechanism. The benzene rings of the drugs as well as their aromatic heterocyclic rings are expected to interact with the polarized aromatic rings on carbons via the mechanism of pi-pi electron coupling [28,55]. Additionally, the Lewis acid–base interaction, where the amino groups of PRM molecules are the Lewis bases and the O-

containing groups of carbons serve as Lewis acids, may be another important mechanism of adsorption of PRM. The presence of lone pairs of electrons on nitrogen atoms produces dipolar moments for PRM. Negative charges are close to these nitrogen atoms and the presence of the polar oxygen groups on the carbon surface with a lone pair of electrons on their oxygen atoms may be the reason for surface specific interactions between the oxygen surface groups of carbon samples and PRM molecules [28]. The latter was in accordance with another study [28], in which the adsorbent material was activated carbon produced from potato peels and the pollutants adsorbed were pharmaceutical compounds (pramipexole and dorzolamide).

3.2.2. Equilibrium/Isotherms

Figure 10 depicts the curves of the isotherms for the pramipexole adsorption from aqueous solutions. Additionally, the isothermal parameters that resulted from the experimental data fitting of Langmuir and Freundlich models are reported in Table 3.

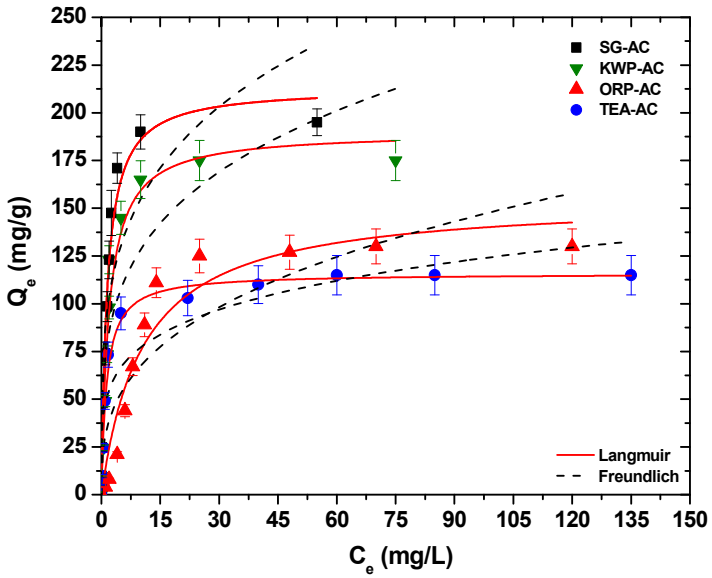

Figure 10. Isotherms of all AC samples at 25 °C.

Table 3. Equilibrium parameters for the adsorption of PRM onto AC samples.

	Langmuir Equation			Freundlich Equation		
Material	Q_m mg/g	K_L L/mg	R^2	K_F $mg^{1-1/n}$ $L^{1/n}$ g^{-1}	n	R^2
SG-AC	213	0.678	0.984	87.66	4.047	0.793
ORP-AC	155	0.094	0.929	47.73	4.800	0.856
TEA-AC	115	0.744	0.986	30.58	2.917	0.783
KWP-AC	190	0.517	0.968	72.02	3.988	0.788

The obtained correlation coefficients (R^2) from the Langmuir model ranged from 0.929 to 0.986, while those of the Freundlich model ranged from 0.783 to 0.856. The Langmuir model fits the experimental results of all AC samples better.

As it can be observed, the highest pramipexole adsorption capacity (Q_{max}) at 25 °C was achieved with the use of SG-AC and KWP-AC (Table 3) at pH 3. Therefore, the adsorption capacity order found was $Q_{max,SG\text{-}AC} > Q_{max,KWPs\text{-}AC} > Q_{max,ORP\text{-}AC} > Q_{max,TEA\text{-}AC}$, respectively. The aforementioned order is in accordance with the surface area order (Table 2), suggesting the key role of the specific surface area for PRM removal. This can be supported by study of the correlation of the maximum adsorption capacity with the surface area (Figure 11). As it can be observed, an increment of the specific surface area is

accompanied by a non-linear increase of the removal efficiency, suggesting that except the specific surface area, the size and shape of the pores as well as the surface chemistry matter. It is worth mentioning that no trend was observed between the remaining textural features and the adsorption capacity. The equilibrium PRM uptake in the case of all synthesized AC samples was affected by the initial concentration of PRM using a constant dosage of adsorbent (1 g/L). For low concentrations (10–100 mg/g), the adsorption of PRM using the AC adsorbents was very intense and reached the phase of equilibrium rapidly. This phenomenon indicates the possibility of forming monolayer coverage of PRM molecules on the outer interface of the AC samples. Additionally, the size of the pores and their network favors the diffusion of the PRM molecules towards the adsorption active sites. For higher concentrations (100–250 mg/g), the highest Q_{max} of SG-AC may indicate the formation of multilayer coverage due to a higher amount of oxygen groups; the same is also presented for all AC samples but with lower Q_{max}. Table 4 shows the parameters calculated from the error analysis.

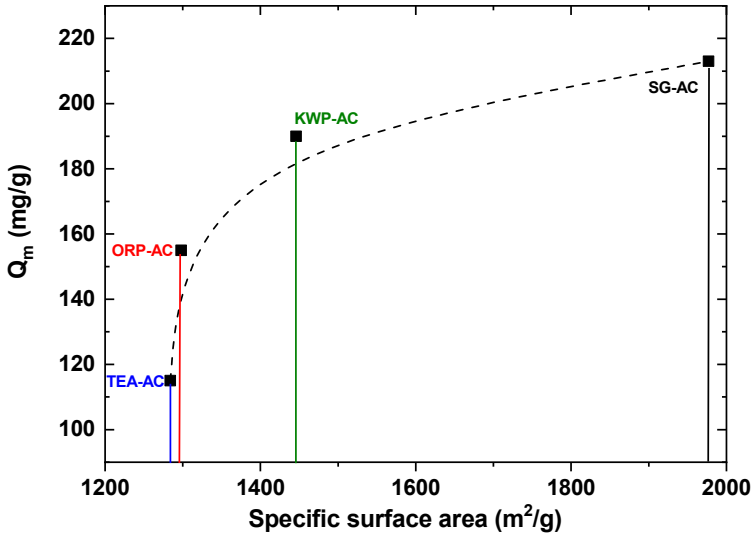

Figure 11. Dependence of the PRM adsorption capacity on the specific surface area.

Table 4. The values of three different error analyses of isotherm models for adsorption of PRM onto AC samples.

	Langmuir Equation			Freundlich Equation		
Material	**SSE**	**SAE**	**ARE (%)**	**SSE**	**SAE**	**ARE (%)**
SG-AC	855.91	77.79	6.00	11,271.08	321.99	18.30
ORP-AC	2145.58	136.67	9.66	6249.45	231.14	18.59
TEA-AC	320.24	45.33	2.39	3210.60	160.77	11.77
KWP-AC	1516.85	101.45	6.41	10,359.94	324.92	20.01

A direct comparison among the value of Q_{max} of various adsorbent materials cannot be objective due to the different parameters of the followed synthetic protocols (temperature, activation agent, cost of the precursor, etc.), and also mainly to the cost of synthesis. However, to obtain a first sense about the range of adsorption of the used AC samples, some examples are given in Table 5. As it can be observed, SG-AC has an excellent adsorption capacity when compared with other adsorbent materials, and more importantly compared to other carbonaceous materials obtained from biomass like potato peels or tea waste.

Table 5. Maximum adsorption capacities of different adsorbent materials for the removal of pharmaceuticals from aqueous solutions.

Adsorbent	Compound	Q_{max} (mg/g)	References
Nanoporous carbon derived from MOFs	Ciprofloxacin	417	[56]
MWNTs with 4.7% oxygen content	Ciprofloxacin	206	[57]
Graphene oxide	Ciprofloxacin	379	[58]
Porous graphene hydrogel granules	Ciprofloxacin	236	[59]
Graphene oxide	Sulfamethoxazole	240	[58]
High-silica zeolite HSZ-385	Sulfathiazole	402	[28]
Tea waste biochars	Sulfamethazine	34	[60]
Graphene oxide	Tetracyclines	313	[61]
Sulfonate grafted chitosan	Pramipexole	337	[62]
N-(2-carboxybenzyl) grafted chitosan	Pramipexole	307	[62]
Non-grafted cross-linked chitosan	Pramipexole	181	[62]
Activated carbon from potato peels (hydrothermal)	Pramipexole	66	[28]
Activated carbon from potato peels (pyrolyzed)	Pramipexole	56	[28]
SG-AC	Pramipexole	213	This study
KWP-AC	Pramipexole	190	This study
ORP-AC	Pramipexole	155	This study
TEA-AC	Pramipexole	115	This study

4. Conclusions and Perspectives

The synthesis of activated carbon derived from sucrose, as a carbonaceous precursor, gave an excellent yield (~58%) with a mesoporous structure (~59.3%) at a very low impregnation ratio of the activation agent (H_3PO_4) per SG (1.7:1). According to nitrogen physisorption tests, the activated carbon derived from sucrose had the highest surface area (1977 m^2/g) with the total pores volume, mesopores volume, and external surface area being 1.382 cm^3/g, 0.819 cm^3/g, and 751 m^2/g, respectively. It is worth noting that the other synthetic protocols require a prolonged duration for the preparation of AC before pyrolysis and higher energy consumption, when compared with the synthesis of sucrose activated carbon. The effect of the initial PRM concentration was studied and the equilibrium results (isotherms) fitted the Langmuir model better. The adsorption capacities were found to be 213, 190, 155, and 115 mg/g for AC samples produced from sucrose, kiwi peels, orange peels, and tea stalks, respectively. The optimum pramipexole dihydrochloride removal in the case of sucrose activated carbon was found to be 95% for pH 3 at a temperature of 25 °C. A future work may be the pyrolysis yielded after chemical impregnation of sucrose-activated carbon in a microwave oven, autoclave, or other devices at 350–800 °C or higher, under N_2 flow. It may also be worthy to study the combination of other different activation agents (acids or bases).

Author Contributions: Methodology, E.V.L., K.R., D.A.G., A.C.M. and G.Z.K.; writing—original draft preparation, E.V.L., K.R., D.A.G., A.C.M. and G.Z.K.; writing—review and editing, E.V.L., K.R., D.A.G., A.C.M. and G.Z.K.; Supervision, G.Z.K. All authors have read and agreed to the published version of the manuscript.

Funding: This research was funded by the Greek Ministry of Development and Investments (General Secretariat for Research and Technology) through the research project "Intergovernmental International Scientific and Technological Innovation-Cooperation. Joint declaration of Science and Technology Cooperation between China and Greece" with the topic "Development of monitoring and removal strategies of emerging micro-pollutants in wastewaters" (Grant no: T7ΔKI-00220).

Institutional Review Board Statement: Not applicable.

Informed Consent Statement: Not applicable.

Data Availability Statement: The raw/processed data required to reproduce these findings can be shared if required.

Conflicts of Interest: The authors declare that they have no known competing financial interests or personal relationships that could have appeared to influence the work reported in this article.

References

1. Liou, T.-H. Development of mesoporous structure and high adsorption capacity of biomass-based activated carbon by phosphoric acid and zinc chloride activation. *Chem. Eng. J.* **2010**, *158*, 129–142. [CrossRef]
2. Acosta, L.; Galeano-Caro, D.; Medina, O.E.; Cortés, F.B.; Franco, C.A. Nano-Intermediate of Magnetite Nanoparticles Supported on Activated Carbon from Spent Coffee Grounds for Treatment of Wastewater from Oil Industry and Energy Production. *Processes* **2020**, *9*, 63. [CrossRef]
3. Alam Ashik, M.; Hossain, A.; Hossain, D.; Johir, M.; Hossen, J.; Rahman, S.; Zhou, J.L.; Hasan, A.K.; Karmakar, A.K.; Ahmed, M.B. The Potentiality of Rice Husk-Derived Activated Carbon: From Synthesis to Application. *Processes* **2020**, *8*, 203. [CrossRef]
4. Filho, A.V.; Kulman, R.X.; Tholozan, L.V.; De Almeida, A.R.F.; Da Rosa, G.S. Preparation and Characterization of Activated Carbon Obtained from Water Treatment Plant Sludge for Removal of Cationic Dye from Wastewater. *Processes* **2020**, *8*, 1549. [CrossRef]
5. Hira, S.A.; Yusuf, M.; Annas, D.; Hui, H.S.; Park, K.H. Biomass-derived activated carbon as a catalyst for the effective degradation of Rhodamine B dye. *Processes* **2020**, *8*, 926. [CrossRef]
6. Zhang, H.; Yan, Y.; Yang, L. Preparation of activated carbon from sawdust by zinc chloride activation. *Adsorption* **2010**, *16*, 161–166. [CrossRef]
7. Khelfa, A.; Rodrigues, F.A.; Koubaa, M.; Vorobiev, E. Microwave-Assisted Pyrolysis of Pine Wood Sawdust Mixed with Activated Carbon for Bio-Oil and Bio-Char Production. *Processes* **2020**, *8*, 1437. [CrossRef]
8. León, M.; Silva, J.; Carrasco, S.; Barrientos, N. Design, cost estimation and sensitivity analysis for a production process of activated carbon fromwaste nutshells by physical activation. *Processes* **2020**, *8*, 945. [CrossRef]
9. Liu, Y.; Cheng, H.; He, Y. Application and Mechanism of Sludge-Based Activated Carbon for Phenol and Cyanide Removal from Bio-Treated Effluent of Coking Wastewater. *Processes* **2020**, *8*, 82. [CrossRef]
10. Ahmadpour, A.; Do, D. The preparation of activated carbon from macadamia nutshell by chemical activation. *Carbon* **1997**, *35*, 1723–1732. [CrossRef]
11. Rashidi, N.F.D.; Jamali, N.S.; Mahamad, S.S.; Ibrahim, M.F.; Abdullah, N.; Ismail, S.F.; Izhar, S. Effects of Alginate and Chitosan on Activated Carbon as Immobilisation Beads in Biohydrogen Production. *Processes* **2020**, *8*, 1254. [CrossRef]
12. Yang, H.-C.; Lee, M.-W.; Eun, H.-C.; Kim, H.-J.; Lee, K.; Seo, B.-K. Thermal Decontamination of Spent Activated Carbon Contaminated with Radiocarbon and Tritium. *Processes* **2020**, *8*, 1359. [CrossRef]
13. Ziganshina, E.E.; Belostotskiy, D.E.; Bulynina, S.S.; Ziganshin, A.M. Influence of Granular Activated Carbon on Anaerobic Co-Digestion of Sugar Beet Pulp and Distillers Grains with Solubles. *Processes* **2020**, *8*, 1226. [CrossRef]
14. Anastopoulos, I.; Kyzas, G.Z. Agricultural peels for dye adsorption: A review of recent literature. *J. Mol. Liq.* **2014**, *200*, 381–389. [CrossRef]
15. Heidarinejad, Z.; Dehghani, M.H.; Heidari, M.; Javedan, G.; Ali, I.; Sillanpää, M. Methods for preparation and activation of activated carbon: A review. *Environ. Chem. Lett.* **2020**, *18*, 393–415. [CrossRef]
16. Luo, Y.; Guo, W.; Ngo, H.H.; Nghiem, L.D.; Hai, F.I.; Zhang, J.; Liang, S.; Wang, X.C. A review on the occurrence of micropollutants in the aquatic environment and their fate and removal during wastewater treatment. *Sci. Total Environ.* **2014**, *473*, 619–641. [CrossRef]
17. Kurniawan, T.A.; Chan, G.Y.; Lo, W.-H.; Babel, S. Physico–chemical treatment techniques for wastewater laden with heavy metals. *Chem. Eng. J.* **2006**, *118*, 83–98. [CrossRef]
18. Busca, G.; Berardinelli, S.; Resini, C.; Arrighi, L. Technologies for the removal of phenol from fluid streams: A short review of recent developments. *J. Hazard. Mater.* **2008**, *160*, 265–288. [CrossRef]
19. Nabil, G.M.; El-Mallah, N.M.; Mahmoud, M.E. Enhanced decolorization of reactive black 5 dye by active carbon sorbent-immobilized-cationic surfactant (AC-CS). *J. Ind. Eng. Chem.* **2014**, *20*, 994–1002. [CrossRef]
20. Chong, M.N.; Jin, B.; Chow, C.W.; Saint, C. Recent developments in photocatalytic water treatment technology: A review. *Water Res.* **2010**, *44*, 2997–3027. [CrossRef]
21. Chenab, K.K.; Sohrabi, B.; Jafari, A.; Ramakrishna, S. Water treatment: Functional nanomaterials and applications from adsorption to photodegradation. *Mater. Today Chem.* **2020**, *16*, 100262. [CrossRef]
22. Pandey, S.; Spiro, E.F.; Waanders, F.; Kumar, N.; Ray, S.S.; Kim, J.; Kang, M. Equilibrium, kinetic, and thermodynamic studies of lead ion adsorption from mine wastewater onto MoS2-clinoptilolite com-posite. *Mater. Today Chem.* **2020**, *18*, 100376. [CrossRef]
23. Santoso, E.; Ediati, R.; Kusumawati, Y.; Bahruji, H.; Sulistiono, D.; Prasetyoko, D. Review on recent advances of carbon based adsorbent for methylene blue removal from waste water. *Mater. Today Chem.* **2020**, *16*, 100233. [CrossRef]
24. Sharma, M.; Poddar, M.; Gupta, Y.; Nigam, S.; Avasthi, D.; Adelung, R.; Abolhassani, R.; Fiutowski, J.; Joshi, M.; Mishra, Y.K. Solar light assisted degradation of dyes and adsorption of heavy metal ions from water by CuO–ZnO tetrapodal hybrid nanocomposite. *Mater. Today Chem.* **2020**, *17*, 100336. [CrossRef]
25. Mohanty, K.; Naidu, J.T.; Meikap, B.C.; Biswas, M.N. Removal of Crystal Violet from Wastewater by Activated Carbons Prepared from Rice Husk. *Ind. Eng. Chem. Res.* **2006**, *45*, 5165–5171. [CrossRef]

26. Yorgun, S.; Yıldız, D. Preparation and characterization of activated carbons from Paulownia wood by chemical activation with H3PO4. *J. Taiwan Inst. Chem. Eng.* **2015**, *53*, 122–131. [CrossRef]
27. Wang, J.; Kaskel, S. KOH activation of carbon-based materials for energy storage. *J. Mat. Chem.* **2012**, *22*, 23710–23725. [CrossRef]
28. Kyzas, G.Z.; Deliyanni, E.A. Modified activated carbons from potato peels as green environmental-friendly ad–Sorbents for the treatment of pharmaceutical effluents. *Chem. Eng. Res. Des.* **2015**, *97*, 135–144. [CrossRef]
29. Lees, J.A.; Hardy, J.; Revesz, T. Parkinson's disease. *Lancet* **2009**, *373*, 2055–2066. [CrossRef]
30. Barone, P.; Poewe, W.; Albrecht, S.; Debieuvre, C.; Massey, D.; Rascol, O.; Tolosa, E.; Weintraub, D. Pramipexole for the treatment of depressive symptoms in patients with Parkinson's disease: A randomised, double-blind, place-bo-controlled trial. *Lancet Neurol.* **2010**, *9*, 573–580. [CrossRef]
31. Allen, R.P.; Picchietti, D.; Hening, W.A.; Trenkwalder, C.; Walters, A.S.; Montplaisi, J. Restless legs syndrome: Diagnostic criteria, special considerations, and epidemiology: A report from the restless legs syndrome diagnosis and epidemiology workshop at the National Institutes of Health. *Sleep Med.* **2003**, *4*, 101–119. [CrossRef]
32. Fernandez, M.E.; Nunell, G.V.; Bonelli, P.R.; Cukierman, A.L. Activated carbon developed from orange peels: Batch and dynamic competitive adsorption of basic dyes. *Ind. Crops Prod.* **2014**, *62*, 437–445. [CrossRef]
33. Kurniawan, T.A.; Chan, G.Y.; Lo, W.-H.; Babel, S. Comparisons of low-cost adsorbents for treating wastewaters laden with heavy metals. *Sci. Total Environ.* **2006**, *366*, 409–426. [CrossRef] [PubMed]
34. Hussain, S. Waste tea as a novel adsorbent: A review. *Appl. Water Sci.* **2018**, *8*, 1–16. [CrossRef]
35. Sandoval, R.; Cooper, A.M.; Aymar, K.; Jain, A.; Hristovski, K. Removal of arsenic and methylene blue from water by granular activated carbon media impregnated with zirconium dioxide nanoparticles. *J. Hazard. Mater.* **2011**, *193*, 296–303. [CrossRef]
36. Guo, Y.; Qi, P.S.; Liu, Y.Z. A Review on Advanced Treatment of Pharmaceutical Wastewater. *IOP Conf. Ser: Earth Environ. Sci.* **2017**, *63*, 012025. [CrossRef]
37. Langmuir, I. The adsorption of gases on plane surfaces of glass, mica and platinum. *J. Am. Chem. Soc.* **1918**, *40*, 1361–1403. [CrossRef]
38. Freundlich, H. Over the adsorption in solution. *Z. Phys. Chem.* **1906**, *57*, 385–470.
39. Puzii, A.M. Methods of production, structure, and physicochemical characteristics of phosphorylated carbon adsorbents. *Theor. Exp. Chem.* **2011**, *47*, 277–291. [CrossRef]
40. El-Hendawy, A.-N.A. Variation in the FTIR spectra of a biomass under impregnation, carbonization and oxi-dation conditions. *J. Analy. Appl. Pyrol.* **2006**, *75*, 59–166.
41. Liu, Q.-S.; Zheng, T.; Wang, P.; Guo, L. Preparation and characterization of activated carbon from bamboo by microwave-induced phosphoric acid activation. *Ind. Crop. Prod.* **2010**, *31*, 233–238. [CrossRef]
42. Mohammadi, S.Z.; Karimi, M.A.; Afzali, D.; Mansouri, F. Removal of Pb(II) from aqueous solutions using activated carbon from Sea-buckthorn stones by chemical activation. *Desalination* **2010**, *262*, 86–93. [CrossRef]
43. Liu, H.; Wang, X.; Zhai, G.; Zhang, J.; Zhang, C.; Bao, N.; Cheng, C. Preparation of activated carbon from lotus stalks with the mixture of phosphoric acid and pentaerythritol impregnation and its application for Ni(II) sorption. *Chem. Eng. J.* **2012**, *209*, 155–162. [CrossRef]
44. Kyzas, G.Z.; Deliyanni, E.A.; Matis, K.A. Activated carbons produced by pyrolysis of waste potato peels: Cobalt ions removal by adsorption. *Colloids Surfaces A Physicochem. Eng. Asp.* **2016**, *490*, 74–83. [CrossRef]
45. Huang, Y.; Ma, E.; Zhao, G. Thermal and structure analysis on reaction mechanisms during the preparation of activated carbon fibers by KOH activation from liquefied wood-based fibers. *Ind. Crops Prod.* **2015**, *69*, 447–455. [CrossRef]
46. Huang, L.; Sun, Y.; Wang, W.; Yue, Q.; Yang, T. Comparative study on characterization of activated carbons prepared by microwave and conventional heating methods and application in removal of oxytetracycline (OTC). *Chem. Eng. J.* **2011**, *171*, 1446–1453. [CrossRef]
47. Sulistianti, I.; Krisnandi, Y.K.; Moenandar, I. Study of CO2 adsorption capacity of mesoporous carbon and activated carbon modified by triethylenetetramine (TETA). *IOP Conf. Ser. Mat. Sci. Eng.* **2017**, *188*, 012041. [CrossRef]
48. Wang, Y.-T.; Lu, A.-H.; Zhang, H.-L.; Li, W.-C. Synthesis of Nanostructured Mesoporous Manganese Oxides with Three-Dimensional Frameworks and Their Application in Supercapacitors. *J. Phys. Chem. C* **2011**, *115*, 5413–5421. [CrossRef]
49. Thommes, K.; Kaneko, A.V.; Neimark, J.P.; Olivier, F.; Rodriguez-Reinoso, J.; Rouquerol, K.S.W. Sing, Phy-sisorption of gases, with special reference to the evaluation of surface area and pore size distribution (IUPAC Tech-nical Report). *Pure Appl. Chem.* **2015**, *87*, 1051–1069. [CrossRef]
50. Chandra, T.C.; Mirna, M.M.; Sunarso, J.; Sudaryanto, Y.; Ismadji, S. Activated carbon from durian shell: Prepa-ration and characterization. *J. Taiwan Inst. Chem. Eng.* **2009**, *40*, 457–462. [CrossRef]
51. Molina-Sabio, M.; Rodriguez-Reinoso, F. Role of chemical activation in the development of carbon porosity. *Colloids Surf. A Physicochem. Eng. Aspects* **2004**, *241*, 15–25. [CrossRef]
52. Kaipannan, S.; Nagarajan, S.; Manickavasakam, K.; Sathish, M. Orange Peel Derived Activated Carbon for Fab-rication of High-Energy and High-Rate Supercapacitors. *ChemistrySelect* **2017**, *2*, 11384–11392.
53. Rivas-Cantu, R.C.; Mills, P.L.; Jones, K.D. A citrus waste-based biorefinery as a source of renewable energy: Technical advances and analysis of engineering challenges. *Waste Manag. Res.* **2013**, *31*, 413–420. [CrossRef] [PubMed]
54. Ye, J.; Jin, J.; Liang, H.; Lu, J.; Du, Y.; Zheng, X.; Liang, Y.-R. Using tea stalk lignocellulose as an adsorbent for separating decaffeinated tea catechins. *Bioresour. Technol.* **2009**, *100*, 622–628. [CrossRef] [PubMed]

55. Ji, L.; Chen, W.; Zheng, S.; Xu, Z.; Zhu, D. Adsorption of Sulfonamide Antibiotics to Multiwalled Carbon Nano-tubes. *Langmuir* **2009**, *25*, 11608–11613. [CrossRef] [PubMed]
56. Li, S.; Zhang, X.; Huang, Y. Zeolitic imidazolate framework-8 derived nanoporous carbon as an effective and recyclable adsorbent for removal of ciprofloxacin antibiotics from water. *J. Hazard. Mater.* **2017**, *321*, 711–719. [CrossRef]
57. Yu, F.; Sun, S.; Han, S.; Zheng, J.; Ma, J. Adsorption removal of ciprofloxacin by multi-walled carbon nanotubes with different oxygen contents from aqueous solutions. *Chem. Eng. J.* **2016**, *285*, 588–595. [CrossRef]
58. Chen, H.; Gao, B.; Li, H. Removal of sulfamethoxazole and ciprofloxacin from aqueous solutions by graphene oxide. *J. Hazard. Mater.* **2015**, *282*, 201–207. [CrossRef]
59. Ma, J.; Yang, M.; Yu, F.; Zheng, J. Water-enhanced Removal of Ciprofloxacin from Water by Porous Graphene Hydrogel. *Sci. Rep.* **2015**, *5*, srep13578. [CrossRef]
60. Rajapaksha, A.U.; Vithanage, M.; Zhang, M.; Ahmad, M.; Mohan, D.; Chang, S.X.; Ok, Y.S. Pyrolysis condition affected sulfamethazine sorption by tea waste biochars. *Bioresour. Technol.* **2014**, *166*, 303–308. [CrossRef]
61. Gao, Y.; Li, Y.; Zhang, L.; Huang, H.; Hu, J.; Shah, S.M.; Su, X. Adsorption and removal of tetracycline antibiotics from aqueous solution by graphene oxide. *J. Colloid Interface Sci.* **2012**, *368*, 540–546. [CrossRef] [PubMed]
62. Kyzas, G.Z.; Kostoglou, M.; Lazaridis, N.K.; Lambropoulou, D.A.; Bikiaris, D.N. Environmental friendly tech-nology for the removal of pharmaceutical contaminants from wastewaters using modified chitosan adsorbents. *Chem. Eng. J.* **2013**, *222*, 248–258. [CrossRef]